Rayleigh scattering in an emitter-nanofiber-coupling system

Shui-Jing Tang, Fei Gao, Da Xu, Yan Li, Qihuang Gong, and Yun-Feng Xiao*
State Key Laboratory for Mesoscopic Physics and School of Physics, Peking University; Collaborative Innovation Center of Quantum Matter, Beijing 100871, People's Republic of China
(Received 6 December 2016; published 3 April 2017)

Scattering is a general process in both fundamental and applied physics. In this paper, we investigate Rayleigh scattering of a solid-state-emitter coupled to a nanofiber, by S-matrix-like theory in k-space description. Under this model, both Rayleigh scattering and dipole interaction are studied between a two-level artificial atom embedded in a nanocrystal and fiber modes (guided and radiation modes). It is found that Rayleigh scattering plays a critical role in the transport properties and quantum statistics of photons. On the one hand, Rayleigh scattering produces the transparency in the optical transmitted field of the nanofiber, accompanied by the change of atomic phase, population, and frequency shift. On the other hand, the interference between two kinds of scattering fields by Rayleigh scattering and dipole transition modifies the photon statistics (second-order autocorrelation function) of output fields, showing a strong wavelength dependence. This study provides guidance for the solid-state emitter acting as a single-photon source and can be extended to explore the scattering effect in many-body physics.

DOI: 10.1103/PhysRevA.95.043801

I. INTRODUCTION

The strong coupling between light and matter has been realized in waveguide-based quantum electrodynamics (wQED), which has attracted much attention recently in quantum physics and quantum information science [1,2]. Compared to cavity-QED systems [3], wQED offers two new features: the existence of a continuum of states and the confined one-dimensional phase space, together bringing in new physical effects. In the pioneering work, a single atom coupled to a waveguide is investigated, which reveals modulated spontaneous emission of the atom [4–9]. Further, the photon coherent transport properties are strongly modified owing to the enhanced spontaneous emission [10]. As for many-body physics, the light-induced correlation effects between atoms reveal many interesting phenomena, such as cooperative Lamb shift [11,12] and superradiant effects [13].

Besides the atomic wQED, solid-state alternatives have attracted great interest in recent years. Solid-state wQED has the obvious experimental asset that the elaborate experimental techniques for trapping and cooling single atoms are not required [14]. Solid-state quantum emitters—including color defects in diamond [15–17] and semiconductor quantum dots [18–20]—have turned out to be very promising candidates for realizing single-photon sources and quantum information processing [21–23]. A different feature of solid-state quantum emitters is that they are embedded inside classical nanocrystals, whose sizes are typically much larger than the neutral atoms and ions used in conventional QED systems. Thus, in addition to the dipole interaction between the atom and waveguide modes, the classical nanocrystal may produce a strong scattering interaction [24–29].

In this paper, we investigate Rayleigh scattering in a solid-state wQED. An S-matrix-like theory in k-space description is built to study the photon transport properties and quantum statistical behaviors, by considering both the classical Rayleigh scattering and quantum dipole transition. Taking both guided and radiation modes of nanofiber into account in the weak-driving optical field, induced transparency appears in the transmission spectrum in the presence of strong Rayleigh scattering. This transparent phenomenon occurs owing to the complete destructive interference between two kinds of scattering fields by Rayleigh scattering and dipole transition. Rayleigh scattering can also alter the spectroscopic properties of atoms, such as the atomic phase, population, and resonant frequency, depending strongly on the nanocrystal size and atomic dipole moment. Moreover, the photon statistics (second-order autocorrelation function) of output fields show a strong wavelength dependence, especially on the reflected field, owing to the Lorentz spectroscopic properties of atoms and the interference between two kinds of scattering fields.

II. MODEL

Figure 1(a) sketches the coupling system, in which a solid-state quantum emitter—a two-level artificial atom embedded in a nanocrystal (radius: a)—is placed in the vicinity of a nanofiber. A monochromatic coherent light propagates through the nanofiber and interacts with the emitter. The cylindrical coordinates (ρ,ϕ,z) are shown in Fig. 1(a) with z the axis of the nanofiber. The electric field of nanofiber can be expanded in the guided and radiation modes, and the positive-frequency component of the electric field is given by $\boldsymbol{E}^{(+)}=\sum_{\boldsymbol{k}}\boldsymbol{E}_{\boldsymbol{k}}a_{\boldsymbol{k}}e^{-i\omega_k t}$. Here $a_{\boldsymbol{k}}$ ($a_{\boldsymbol{k}}^{\dagger}$) denotes the annihilation (creation) operator of the fiber modes, with wave vector $\boldsymbol{k}$. The amplitude of the guided mode is $\boldsymbol{E}_g=\sqrt{\hbar\omega_k/(2\varepsilon_0\varepsilon_1 L_g)}\boldsymbol{u}(\boldsymbol{\rho})e^{i\boldsymbol{k}\cdot\boldsymbol{z}}$, with the electric-field profile function $\boldsymbol{u}(\boldsymbol{\rho})$ satisfying the normalized condition $\int_0^{2\pi}d\phi\int_0^{\infty}n^2\boldsymbol{u}^*(\boldsymbol{\rho})\cdot\boldsymbol{u}(\boldsymbol{\rho})\rho d\rho=1$ (Refs. [8,30]). As for the radiation vacuum modes, the amplitude is given by $\boldsymbol{E}_v=\sqrt{\hbar\omega_k/(2\varepsilon_0\varepsilon_1 V_v)}e^{i\boldsymbol{k}\cdot\boldsymbol{r}}\hat{\boldsymbol{e}}_v$ (here $\boldsymbol{r}=\rho\boldsymbol{e}_\rho+z\boldsymbol{e}_z$) (Ref. [24]). The $\hat{\boldsymbol{e}}_v$ denotes the basis vector of radiation mode; L_g and V_v are the quantized length of the guided modes and the quantized volume of the radiation vacuum modes, respectively; n represents the step-index profile of the nanofiber; ε_0 is the electric permittivity of the vacuum, and $\varepsilon_1=1$ denotes

*Corresponding author: yfxiao@pku.edu.cn; www.phy.pku.edu.cn/~yfxiao/index.html

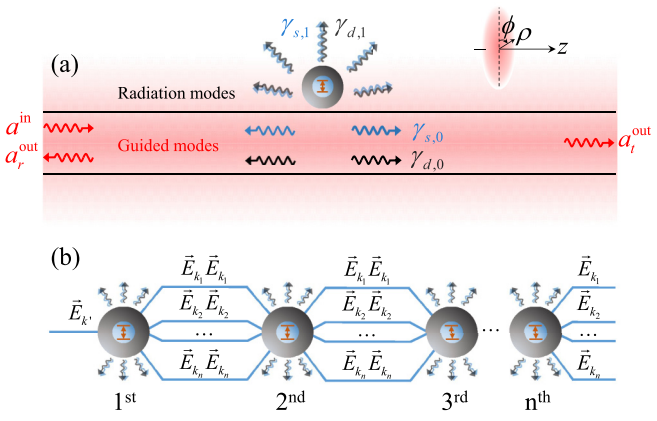

FIG. 1. (a) Schematic illustration of the system composed of a nanofiber and a solid-state emitter (a two-level artificial atom embedded in a nanocrystal). (b) The n-times scattering process diagram. The excited input mode $E_{k'}$ is scattered into other guided or radiation modes E_{k_j} $(j = 1,2,\ldots,n)$ by the emitter, through Rayleigh scattering and atomic dipole transition with strength $p_s + p_d$. Subsequently, each mode propagates described by transmission matrix N. The two procedures take place repeatedly n times.

the relative permittivity of the surrounding medium (vacuum here).

The solid-state emitter interacts with the fiber modes by two optical pathways: Rayleigh scattering by the nanocrystal itself and the dipole transition of the two-level artificial atom. Rayleigh scattering of a subwavelength scatter can be modeled by the dipole approximation [31]. The electric field of the input fiber modes $\boldsymbol{k}'$ induces a dipole moment $\boldsymbol{P}_{\rm sca} = \varepsilon_0\alpha\boldsymbol{E}_{\boldsymbol{k}'}$ in the nanocrystal, which is similar to the intrinsic dipole moment of the atom. The $\alpha = 4\pi a^3(\varepsilon_d - \varepsilon_1)/(\varepsilon_d + 2\varepsilon_1)$ represents the polarizability of the nanocrystal (spherical), and ε_d denotes the relative permittivity of the nanocrystal. Thus, for the emitter-nanofiber-coupling system, under the rotating-wave approximation in the weak-field limit, the Hamiltonian $H = H_s + H_d$ in the interaction picture is given by

$$H_s = \sum_{\boldsymbol{k}\boldsymbol{k}'} \hbar g_{\boldsymbol{k}\boldsymbol{k}'} a_{\boldsymbol{k}}^\dagger a_{\boldsymbol{k}'} e^{i(\omega_{\boldsymbol{k}} - \omega_{\boldsymbol{k}'})t}, \tag{1}$$

$$H_d = \sum_{\boldsymbol{k}} \hbar(G_{\boldsymbol{k}} a_{\boldsymbol{k}}^\dagger \sigma_- e^{i(\omega_{\boldsymbol{k}} - \omega_0)t} + \text{H.c.}). \tag{2}$$

We use the same format for the quantum emitter coupling with both guided modes and radiation vacuum modes in this interaction Hamiltonian. The Hamiltonian H_s describes the nanocrystal-induced scattering into fiber mode fields, where the coupling strength $g_{\boldsymbol{k}\boldsymbol{k}'} = -p_s\boldsymbol{E}_{\boldsymbol{k}}^* \cdot \boldsymbol{E}_{\boldsymbol{k}'}$ with $p_s = \varepsilon_0\varepsilon_1\alpha/\hbar$. The H_d characterizes the dipole interaction between the atom and fiber modes, here the coupling strength $G_{\boldsymbol{k}} = -\boldsymbol{E}_{\boldsymbol{k}}^* \cdot \boldsymbol{P}_{\rm atom}^*/\hbar$ with the intrinsic dipole $\boldsymbol{P}_{\rm atom}$ of the atom. The ω_0 denotes the atomic resonant frequency, and $\sigma_- = |g\rangle\langle e|$ $(\sigma_+ = |e\rangle\langle g|)$ stands for the descending (ascending) operators of the atom.

In the following, we analyze separately Rayleigh scattering of the nanocrystal and the dipole transition of an atom. Then, the interference between the scattering fields by the two coupling pathways is studied to obtain the transmitted and reflected fields. First, Rayleigh scattering in a nanocrystal-nanofiber-coupling system is analyzed from Eq. (1). The equation of motion for the coupled system takes the matrix form

$$\dot{A}^s(t) = M^s(t)A^s(t), \tag{3}$$

where $A^s = [\ a_1; a_2; \cdots; a_{\boldsymbol{k}}; \cdots\ ]$, and the matrix element $M^s_{\boldsymbol{k}\boldsymbol{k}'}(t) = -ig_{\boldsymbol{k}\boldsymbol{k}'}e^{i(\omega_{\boldsymbol{k}} - \omega_{\boldsymbol{k}'})t}$. Based on this equation of motion, we obtain the scattering matrix under the Weisskopf-Wigner approximation, to derive the transition amplitude between arbitrary initial and final states [32], by the input-output relationship $A^s(+\infty) = S^sA^s(-\infty)$. The scattering matrix S^s can be decomposed into $S^s = I + S_1^s + S_2^s + \cdots + S_n^s + \cdots$, where I denotes the identity matrix. The n-times scattering matrix element (given in Appendix A) is

$$\left(S_n^s\right)_{\boldsymbol{k}\boldsymbol{k}'} = 2\pi(ip_s)^n \boldsymbol{E}_{\boldsymbol{k}}^* \cdot N^{n-1} \cdot \boldsymbol{E}_{\boldsymbol{k}'}\delta\omega_{\boldsymbol{k}\boldsymbol{k}'}, \tag{4}$$

where $\delta\omega_{\boldsymbol{k}\boldsymbol{k}'} = \delta(\omega_{\boldsymbol{k}} - \omega_{\boldsymbol{k}'})$, δ is the Kronecker delta. The n-times scattering matrix element $(S_n^s)_{\boldsymbol{k}\boldsymbol{k}'}$ denotes the probability amplitude of the following n-times scattering process [Fig. 1(b)]: In the k-space description, to begin with, the excited input mode $\boldsymbol{k}'$ is scattered into other fiber modes by the nanocrystal with Rayleigh scattering strength p_s. Then, each mode propagates by transmission matrix N. The two procedures take place repeatedly n times, and light field eventually scatters to the output guided or radiation mode $\boldsymbol{k}$. The transmission matrix $N = \pi\sum_{\boldsymbol{k}} \boldsymbol{E}_{\boldsymbol{k}}\boldsymbol{E}_{\boldsymbol{k}}^*\delta\omega_{\boldsymbol{k}\boldsymbol{k}'}$, which is composed of transmission matrices of the guided modes N_g and the radiation modes N_v. Thus, the scattering matrix element of the nanocrystal-nanofiber-coupling system is

$$S^s_{\boldsymbol{k}\boldsymbol{k}'} = \delta_{\boldsymbol{k}\boldsymbol{k}'} + 2i\pi p_s \boldsymbol{E}_{\boldsymbol{k}}^* \cdot (1 - ip_sN)^{-1} \cdot \boldsymbol{E}_{\boldsymbol{k}'}\delta\omega_{\boldsymbol{k}\boldsymbol{k}'}. \tag{5}$$

Second, we turn to study the dipole transition by Eq. (2), and the equations of motion for the atom-nanofiber-coupling system are given by

$$\dot{\sigma}_- = -\sum_{\boldsymbol{k}} iG_{\boldsymbol{k}}^* a_{\boldsymbol{k}} e^{-i(\omega_{\boldsymbol{k}} - \omega_0)t}, \tag{6}$$

$$\dot{a}_{\boldsymbol{k}} = -iG_{\boldsymbol{k}}\sigma_- e^{i(\omega_{\boldsymbol{k}} - \omega_0)t}. \tag{7}$$

Similarly, the equation of motion is expressed in matrix form $\dot{A}^d = M^d(t)A^d$, where $A^d = [\ a_1; a_2; \ldots; a_{\boldsymbol{k}}; \ldots; \sigma_-\ ]$. The matrix element $M^d_{\sigma_-\boldsymbol{k}}(t) = -iG_{\boldsymbol{k}}^* e^{-i(\omega_{\boldsymbol{k}} - \omega_0)t}$ describes the process in which an atom makes a transition from the ground state to the excited state, and a photon of mode $\boldsymbol{k}$ is annihilated. The $M^d_{\boldsymbol{k}\sigma_-}(t) = -iG_{\boldsymbol{k}}e^{i(\omega_{\boldsymbol{k}} - \omega_0)t}$ represents the opposite process. Under the atom-nanofiber-coupling system, fiber modes cannot directly transfer to other fiber modes, thus $M^d_{\boldsymbol{k}\boldsymbol{k}'}(t) = 0$. Under the weak-driving field, the probability amplitude of the one-time scattering process, in which a photon of the fiber mode $\boldsymbol{k}'$ scattered into the fiber mode $\boldsymbol{k}$ by the dipole transition, is described by

$$\int_{-\infty}^{+\infty} dt_1 \int_{-\infty}^{t_1} M_{\boldsymbol{k}\sigma_-}(t_1)M_{\sigma_-\boldsymbol{k}'}(t_2)dt_2 = 2i\pi p_d \boldsymbol{E}_{\boldsymbol{k}}^*\boldsymbol{E}_{\boldsymbol{k}'}\delta\omega_{\boldsymbol{k}\boldsymbol{k}'}, \tag{8}$$

where dipole transition strength $p_d = -\frac{1}{\hbar^2(\omega_{\boldsymbol{k}'} - \omega_0)}\boldsymbol{P}_{\rm atom}\boldsymbol{P}_{\rm atom}$. Similar to the nanocrystal-induced scattering process, after

one-time atom-induced scattering, each mode propagates by the transmission matrix N before the next scattering case.

Finally, for a solid-state emitter, both Rayleigh scattering and atomic dipole transition contribute to the scattering fields. The whole one-time scattering strength in the k-space description is $p_s + p_d$, due to the coherent superposition of the two separated scattering processes. Thus, the input-output relationship for the emitter-nanofiber-coupling system is

$$a_{\boldsymbol{k}}^{\text{out}} = \sum_{\boldsymbol{k}'} \{\delta_{\boldsymbol{k}\boldsymbol{k}'} + 2i\pi \boldsymbol{E}_{\boldsymbol{k}}^{*} \cdot (p_s + p_d) \times [1 - i(p_s + p_d)N]^{-1} \cdot \boldsymbol{E}_{\boldsymbol{k}'} \delta\omega_{\boldsymbol{k}\boldsymbol{k}'}\} a_{\boldsymbol{k}'}^{\text{in}}. \quad (9)$$

For a given input initial-state $\boldsymbol{k}'$, we can calculate the probability amplitude of some desired set of output final-state $\boldsymbol{k}$ by the above formula [Eq. (9)]. Therefore, the transmitted and reflected fields can be obtained for the emitter-nanofiber-coupling system.

III. PHOTON TRANSPORTATION

To simplify the discussion, we assume that the direction of the dipole is parallel to the electric field, and the near-resonant light of different frequencies has the same field distribution. For a linearly polarized incident light with frequency ω, under the Weisskopf-Wigner approximation, the transmission matrices of the guided modes and the radiation modes are $N_g = \frac{\hbar\omega|\boldsymbol{u}(\boldsymbol{\rho})|^2}{2\varepsilon_0\varepsilon_1 v_g} \hat{\boldsymbol{e}}_z \hat{\boldsymbol{e}}^*{}_z$ and $N_v = \frac{\hbar\omega^3}{6\pi\varepsilon_0\varepsilon_1 c^3} I$, respectively (given in Appendix B). The $\hat{\boldsymbol{e}}_z$ and v_g denotes the basis vector of guided modes and the group velocity, respectively. Therefore, the outputs of transmitted and reflected fields are obtained:

$$a_t^{\text{out}} = \frac{\frac{\gamma_{d,1}}{2}(1 - \xi\Delta\omega) - i\Delta\omega}{\frac{\gamma_{d,0}+\gamma_{d,1}}{2}(1 - \xi\Delta\omega) - i\Delta\omega} a^{\text{in}}, \quad (10)$$

$$a_r^{\text{out}} = -\frac{\frac{\gamma_{d,0}}{2}(1 - \xi\Delta\omega)}{\frac{\gamma_{d,0}+\gamma_{d,1}}{2}(1 - \xi\Delta\omega) - i\Delta\omega} a^{\text{in}}. \quad (11)$$

Here $\Delta\omega = \omega - \omega_0$ denotes the detuning of incident light from the atomic resonance. Under the Weisskopf-Wigner approximation, the atom coupled to guided modes and radiation modes can be regarded as a decay of the excited state, described by spontaneous emission rates $\gamma_{d,0}/2 = |\boldsymbol{P}_{\text{atom}}|^2\omega|\boldsymbol{u}(\boldsymbol{\rho})|^2/2\hbar\varepsilon_0\varepsilon_1 v_g$ and $\gamma_{d,1}/2 = |\boldsymbol{P}_{\text{atom}}|^2\omega^3/6\pi\hbar\varepsilon_0\varepsilon_1 c^3$, respectively (given in Appendix B). Similarly, the nanocrystal-induced scattering into the guided and radiation modes can be depicted by Rayleigh scattering rates $\gamma_{s,0}$ and $\gamma_{s,1}$, respectively. The $\xi = \gamma_{s,0}/\gamma_{d,0} = \gamma_{s,1}/\gamma_{d,1} = \alpha\hbar\varepsilon_0\varepsilon_1/|\boldsymbol{P}_{\text{atom}}|^2$ represents the ratio between the Rayleigh scattering rates and the spontaneous emission rates.

By utilizing Eqs. (B3) and (B4), the transmission $\mathcal{T} = \langle a_t^{\text{out}\dagger} a_t^{\text{out}}\rangle/\langle a^{\text{in}\dagger} a^{\text{in}}\rangle$, reflection $\mathcal{R} = \langle a_r^{\text{out}\dagger} a_r^{\text{out}}\rangle/\langle a^{\text{in}\dagger} a^{\text{in}}\rangle$, phase shift $\delta\psi = \text{Arg}[a^{\text{out}}/a^{\text{in}}]$, and loss $\mathcal{L}$ can be determined (given in Appendix B). In the following, as an example, a nitrogen-vacancy (NV) center in diamond, typically treated as a two-level artificial atom at low temperature [27,28,33–35], is considered to analyze the Rayleigh scattering in the emitter-nanofiber-coupling system. Unless otherwise specified, the intrinsic dipole moment of NV center is $|\boldsymbol{P}_{\text{atom}}| = (1.71 \times 10^{-8})e$ cm at the zero-photon line transition $\lambda = 637$ nm, and the diamond nanocrystal has the radius $R = 80$ nm and the relative permittivity $\varepsilon_d = 2.4^2$.

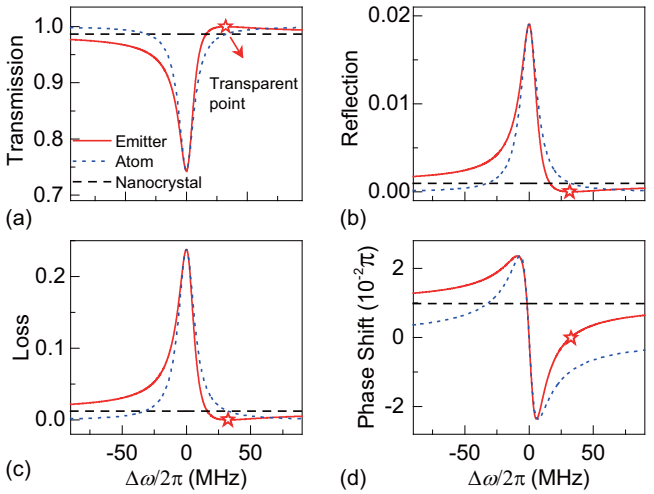

FIG. 2. Transmission $\mathcal{T}$ (a), reflection $\mathcal{R}$ (b), energy loss $\mathcal{L}$ (c), and phase shift $\delta\psi$ (d) of the corresponding transmitted field as a function of the detuning of incident light from the atomic resonance. The following three different cases are plotted: (i) in the absence of the artificial atom ($a = 80$ nm, $|\boldsymbol{P}_{\text{atom}}| = 0$, black dashed curves); (ii) in the absence of the nanocrystal ($a = 0$, $|\boldsymbol{P}_{\text{atom}}| = 1.71 \times 10^{-8}e$ cm, blue dotted curves); and (iii) in the presence of both the two-level atom and nanocrystal ($a = 80$ nm, $|\boldsymbol{P}_{\text{atom}}| = 1.71 \times 10^{-8}e$ cm, red solid curves). The red stars indicate the transparent point at $\Delta\omega = 1/\xi$. The fiber radius is 200 nm and the position of the nanocrystal is ($\rho_0 = 280$ nm, $\phi = 0$, $z = 0$).

The transmission spectra are shown in Fig. 2, under the following three different cases. (i) In the absence of the artificial atom ($a = 80$ nm, $|\boldsymbol{P}_{\text{atom}}| = 0$), Rayleigh scattering of a nanocrystal causes a slight decrease in the fiber transmission, accompanied by the occurrence of the reflection and loss. (ii) In the absence of Rayleigh scattering ($a = 0$, $|\boldsymbol{P}_{\text{atom}}| = 1.71 \times 10^{-8}e$ cm), the transmission spectra show standard Lorenz line shapes, which is consistent with previous results [10]. A difference is that the atom cannot reflect all the on-resonance incident light in the current case, owing to the loss related to the radiation modes (described by $\gamma_{d,1}$). (iii) In the presence of both the Rayleigh scattering and atomic dipole transition ($a = 80$ nm, $|\boldsymbol{P}_{\text{atom}}| = 1.71 \times 10^{-8}e$ cm), owing to the coherent superposition of the two kinds of scattering fields, the transmission spectra show asymmetric Fano line shapes in the near-resonant region, which dramatically deviate from the atom case. At negative detunings, in the k-space description, the phase of scattering field induced by one-time Rayleigh scattering (described by p_s) is same as that by one-time dipole transition (described by p_d). Thus, the constructive interference leads to the stronger scattering into the reflected and radiated fields than that in the absence of Rayleigh scattering, as well as the weaker transmitted field. Similarly, the destructive interference leads to reduced reflection and loss at positive detunings. As a result, an induced transparency point emerges under the complete destructive interference at $\Delta\omega = |\boldsymbol{P}_{\text{atom}}|^2/\alpha\hbar\varepsilon_0\varepsilon_1$, where the transmission $\mathcal{T} = 1$,

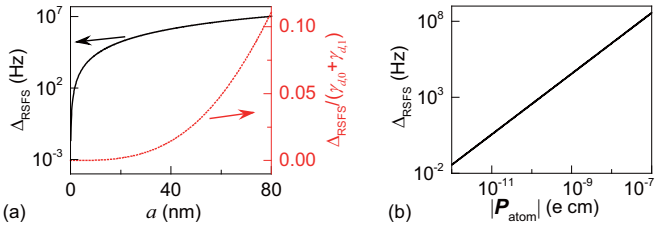

FIG. 3. (a) Rayleigh-scattering-induced resonant frequency shift Δ_{RSFS} of a two-level atom, as a function of the atomic dipole moment $|\boldsymbol{P}_{atom}|$. (b) The shift (black solid curve) and the ratio $\Delta_{RSFS}/(\gamma_{d,1}+\gamma_{d,0})$ (red dotted curve) as a function of radium a of nanocrystal.

reflection $\mathcal{R}=0$, loss $\mathcal{L}=0$, and phase shift of transmitted field $\delta\psi=0$.

IV. ATOMIC RESPONSES

Under the excitation of the optical field, the dipole is thought to perform forced vibration [36]. The nanocrystal-induced scattering perturbs the receptive electric field of the two-level artificial atom, which may affect the spectroscopic properties of the atom, such as the phase, population, and resonant frequency. In order to analyze the atomic responses, the electric field of guided modes is represented by the time-dependent photon operators in the Heisenberg picture $E^{(+)}(z,t)=E_{in}(z,t)+\sum_k E_k e^{i(k\cdot z-\omega_k t)}\int_{-\infty}^{t}\dot{a}_k(\tau)d\tau$, here the excited electric field $E_{in}^{(+)}(z,t)=\sum_k E_k a_k(-\infty)e^{i(k\cdot z-\omega_k t)}$. In the presence of both the dipole transition and Rayleigh scattering, the relationship between the atomic property σ_- and the excited electric field (given in Appendix C) can be obtained:

$$\dot{\sigma}_- = d_0 E_{in}^{(+)}(0,0)e^{-i\Delta\omega t}+d_1\sigma_-, \tag{12}$$

where $d_0=\frac{i|\boldsymbol{P}_{atom}|/\hbar}{1-i(\gamma_{s,1}+\gamma_{s,0})/2}$, $d_1=-\frac{(\gamma_{d,0}+\gamma_{d,1})/2}{1-i(\gamma_{s,1}+\gamma_{s,0})/2}$. The real component of d_1 denotes the decay of the excited state of the atom, and the imaginary component represents the frequency shift induced by Rayleigh scattering (RSFS), which is denoted by

$$\Delta_{RSFS}=\frac{(\gamma_{d,0}+\gamma_{d,1})(\gamma_{s,1}+\gamma_{s,0})}{4+(\gamma_{s,1}+\gamma_{s,0})^2}. \tag{13}$$

It is evident that frequency shift Δ_{RSFS} originates from Rayleigh scattering (described by $\gamma_{s,1},\gamma_{s,0}$). In fact, $\Delta_{RSFS}=0$ in the absence of the Rayleigh scattering. Actually, the frequency shift of an atom placed near a prolate nanospheroid has been reported with the framework of the classical approach in Ref. [37], which points out that the frequency shift is derived from the nanocrystal-induced scattering field. The frequency shift and the ratio between the shift and atomic linewidth are calculated in Fig. 3(a). For a subwavelength scatter, it can be seen that the frequency shift is positively related to the size of the nanocrystal, and the frequency shift reaches as large as one-tenth of the atomic linewidth for a nanocrystal with radius $a=80$ nm. In addition, the frequency shift increases with the square of the intrinsic dipole moment $|\boldsymbol{P}_{atom}|$ in the presence of the Rayleigh scattering, as shown in Fig. 3(a).

We are also interested in phase change of the atom. By considering the oscillatory contribution of the time-dependent operators, the phase change can be obtained via solving

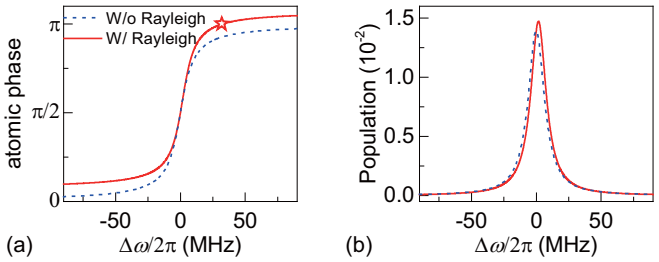

FIG. 4. Phase change of atom (a) and population of the atomic excited state (b) as a function of the detuning $\Delta\omega$, in the absence (blue dotted curves) and presence (red solid curves) of Rayleigh scattering. The input power is 1.5 pW. The red star indicates transparent point $\Delta\omega=1/\xi$.

Eq. (12):

$$\sigma_- = i\frac{1}{\frac{\gamma_{d,0}+\gamma_{d,1}}{2}(1-\xi\Delta\omega)-i\Delta\omega}\sum_k\frac{|\boldsymbol{P}_{atom}|}{\hbar}E_k a_k^{in}. \tag{14}$$

In the weak-driving field, the phase change is shown in Fig. 4(a). An evident translation of the atomic phase can be found in the presence of Rayleigh scattering. Moreover, at the transparency point, $\sigma_-=-\frac{\xi|\boldsymbol{P}_{atom}|}{\hbar}\sum_k E_k a_k^{in}$, indicating a π phase gained by the artificial atom.

The population of the atomic excited state can be calculated by

$$\langle\sigma_+\sigma_-\rangle=\frac{\mathcal{P}\chi}{(\frac{\gamma_{d,0}+\gamma_{d,1}}{2})^2(1-\xi\Delta\omega)^2+(\Delta\omega)^2}, \tag{15}$$

where $\mathcal{P}$ denotes the incident power and $\chi=|\boldsymbol{P}_{atom}|^2|\boldsymbol{u}(\boldsymbol{\rho})|^2/2\hbar^2\varepsilon_0\varepsilon_s v_g$. The population is shown in Fig. 4(b), which reveals Rayleigh scattering plays a minor role as expected.

V. PHOTON STATISTICS OF OUTPUT FIELDS

Since the solid-state quantum emitter is a promising candidate for a single-photon source, here we calculate the second-order correlation functions $g^{(2)}$ of the output (given in Appendix D). For the coherent incident light, the second-order autocorrelation functions of reflected and transmitted fields at zero time delay are shown in Figs. 5(a) and 5(b), respectively.

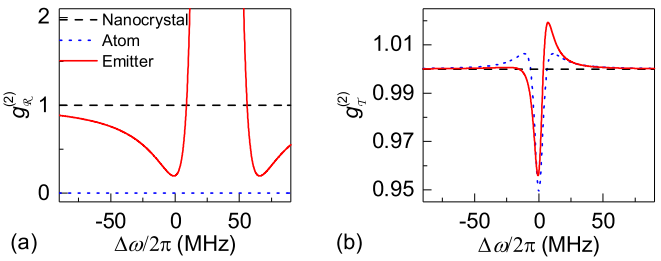

FIG. 5. Second-order autocorrelation function of the reflected field (a) and transmitted field (b). The following three different cases are plotted: (i) in the absence of the two-level artificial atom (black dashed curves); (ii) in the absence of the nanocrystal (blue dotted curves); and (iii) in the presence of both the two-level artificial atom and nanocrystal (red solid curves).

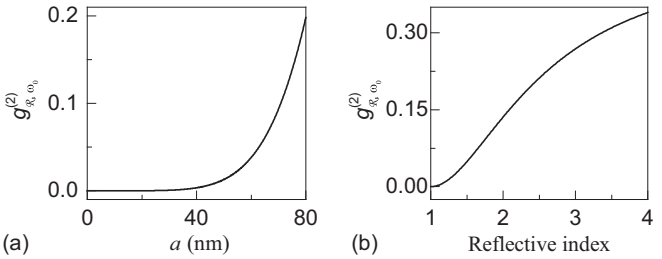

FIG. 6. Second-order autocorrelation function of reflected field of the on-resonance incident optical field $\omega = \omega_0$ as a function of the radius a (a) and refractive index (b) of a nanocrystal.

(i) In the absence of the artificial atom, Rayleigh scattering is a classical effect, which cannot alter the photon quantum statistics feature, as shown by black dashed curves. (ii) In the absence of Rayleigh scattering, as shown by the blue dotted curves, the reflected field originates from the scattering induced by the two-level atom, which cannot emit two photons at once. Therefore, the reflected field shows strong photon blockade effect ($g^{(2)}_{\mathcal{R}} = 0$). The transmitted field has weak photon antibunching phenomenon owing to the weak coupling between the emitter and the nanofiber. (iii) In the presence of both Rayleigh scattering and atomic dipole transition (red solid curves), $g^{(2)}$ shows a strong wavelength dependence. This is due to the interference between the two kinds of scattering fields and the Lorentz spectroscopic properties of atoms, which affects the proportion of quantum fields in output fields.

In the near-resonance region, an antibunching window appears in the second-order autocorrelation spectrum of the reflected field, as shown in Fig. 5(a). The minimum of $g^{(2)}_{\mathcal{R}}$ occurs on resonance ($\Delta\omega = 0$), which depends strongly on the size and refractive index of the nanocrystal [Figs. 6(a) and 6(b)]. It is noted that $g^{(2)}_{\mathcal{R},\omega_0}$ grows slowly until the nanocrystal radius exceeds 40 nm. These phenomena are ascribed to the great change of the nanocrystal polarizability brought on by its size and refractive index [described by $\alpha = 4\pi a^3(\varepsilon_d - \varepsilon_1)/(\varepsilon_d + 2\varepsilon_1)$]. A larger polarizability of nanocrystal increases the contribution of Rayleigh scattering to the reflected field, which degrades the antibunched statistics of reflected photons.

VI. CONCLUSION

In conclusion, we build an S-matrix-like theory in k-space description to investigate Rayleigh scattering of a solid-state quantum emitter coupled to a waveguide. Under this model, both Rayleigh scattering and dipole transition are studied between a two-level artificial atom embedding in a nanocrystal and nanofiber modes (guided and radiation modes). In the weak-driving field, the analytic form of the input-output relationship is obtained to calculate photon transport properties and quantum statistical behaviors. The interference of two kinds of scattering fields predicts interesting physical phenomena. On the one hand, the transparency in the optical transmitted field occurs, accompanied by the atomic phase change, population, and frequency shift. On the other hand, the photon statistics (second-order autocorrelation function) of output fields is strongly modified, showing a wavelength dependence. This work is of importance for the solid-state single-photon source, and can be extended to study the scattering effect in many-body physics.

ACKNOWLEDGMENTS

This project was supported by the Ministry of Science and Technology of China (Grants No. 2016YFA0301302, No. 2013CB921904, and No. 2013CB328704) and the NSFC (Grants No. 61435001, No. 11654003, and No. 11474011). F.G. was supported by the National Fund for Fostering Talents of Basic Science (Grants No. J1030310 and No. J1103205).

APPENDIX A: S-MATRIX OF RAYLEIGH SCATTERING

Rayleigh scattering in a nanocrystal-nanofiber-coupling system is analyzed from Eq. (1). The equation of motion is

$$\dot{a}_{\boldsymbol{k}} = -i \sum_{\boldsymbol{k}'} g_{\boldsymbol{k}\boldsymbol{k}'} a_{\boldsymbol{k}'} e^{i(\omega_{\boldsymbol{k}} - \omega_{\boldsymbol{k}'})t}. \tag{A1}$$

We can write this formula in matrix form

$$\dot{A}^s(t) = M^s(t) A^s(t), \tag{A2}$$

where $A^s = [\ a_1; a_2; \cdots; a_{\boldsymbol{k}}; \cdots\ ]$, and $M^s_{\boldsymbol{k}\boldsymbol{k}'}(t) = -i g_{\boldsymbol{k}\boldsymbol{k}'} e^{i(\omega_{\boldsymbol{k}} - \omega_{\boldsymbol{k}'})t}$. We can solve Eq. (A2) by

$$A^s(+\infty) = A^s(-\infty) + \int_{-\infty}^{+\infty} M^s(\tau) A^s(\tau) d\tau. \tag{A3}$$

The input-output relationship can be obtained by the following iterative formulas:

$$\begin{aligned}
A^s_1 &= A^s(-\infty) + \int_{-\infty}^{+\infty} M^s(t_1) A^s(-\infty) dt_1, \quad A^s_2 = A^s(-\infty) + \int_{-\infty}^{+\infty} M^s(t_2) A^s_1(t_2) dt_2 \\
&= A^s(-\infty) + \int_{-\infty}^{+\infty} M^s(t_2) A^s(-\infty) dt_2 + \int_{-\infty}^{+\infty} M^s(t_2) dt_2 \int_{-\infty}^{t_2} M^s(t_1) dt_1 A^s(-\infty) \cdots \\
A^s_n &= \left[I + \int_{-\infty}^{+\infty} M^s(t_n) dt_n + \cdots + \int_{-\infty}^{+\infty} dt_n \int_{-\infty}^{t_n} dt_{n-1} \ldots \int_{-\infty}^{t_2} M^s(t_n) M^s(t_{n-1}) \ldots M^s(t_1) dt_1 \right] A^s(-\infty) \\
&= \left(I + S^s_1 + S^s_2 + \cdots + S^s_n \right) A^s(-\infty).
\end{aligned} \tag{A4}$$

Thus, we can obtain scattering matrix $A^s(+\infty) = \lim_{n\to\infty} A_n^s = S^s A^s(-\infty)$; here the scattering matrix S^s can be decomposed into $S^s = I + S_1^s + S_2^s + \cdots + S_n^s + \cdots$.

Under the Weisskopf-Wigner approximation, the scattering matrix elements can be calculated by

$$\left(S_1^s\right)_{kk'} = \int_{+\infty}^{-\infty} M_{kk'}^s(t)dt = \int_{-\infty}^{+\infty} -ig_{kk'}e^{i(\omega_k-\omega_{k'})}dt = 2i\pi p_s \vec{E}_k^* \cdot \vec{E}_{k'}\delta(\omega_k - \omega_{k'}), \tag{A5}$$

$$\begin{aligned}\left(S_n^s\right)_{kk'} &= \int_{-\infty}^{+\infty} dt_n \int_{-\infty}^{t_n} dt_{n-1} \ldots \int_{-\infty}^{t_2} M_{kk_n}^s(t_n) M_{k_n k_{n-1}}^s(t_{n-1}) \ldots M_{k_1 k'}^s(t_1)dt_1 \\ &\approx 2(-i\pi)^n \sum_{k_1 k_2 \ldots k_{n-1}} g_{kk_1} g_{k_1 k_2} \cdots g_{k_{n-1}k'} \cdot \delta(\omega_{k_{n-1}} - \omega_{k'})\delta(\omega_{k_{n-2}} - \omega_{k'}) \ldots \delta(\omega_k - \omega_{k'}) \\ &= 2\pi(ip_s)^n \vec{E}_k^* \cdot N^{n-1} \cdot \vec{E}_{k'}\delta(\omega_k - \omega_{k'}),\end{aligned} \tag{A6}$$

where $t_1 < t_2 < \cdots < t_n$, $g_{kk_1}g_{k_1k_2}\cdots g_{k_{n-1}k'} = (-p_s)^n(\vec{E}_k^* \cdot \vec{E}_{k_1})(\vec{E}_{k_1}^* \cdot \vec{E}_{k_2})\ldots(\vec{E}_{k_{n-1}}^* \cdot \vec{E}_{k'})$. Here $(S_n^s)_{kk'}$ denotes the probability amplitude of the n-times scattering process, the mode transmission matrix $N = \pi \sum_k \vec{E}_k \vec{E}_k^* \delta(\omega_k - \omega_{k'})$. Thus, the scattering matrix element of the nanocrystal-nanofiber-coupling system is

$$S_{kk'}^s = \delta_{kk'} + 2i\pi p_s \boldsymbol{E}_k^* \cdot (1 - ip_s N)^{-1} \cdot \boldsymbol{E}_{k'}\delta(\omega_k - \omega_{k'}). \tag{A7}$$

APPENDIX B: THE OUTPUT FIELDS OF THE NANOFIBER

We assume that the direction of the dipole is parallel to the electric field; the near-resonant light of different frequencies has the same field distribution. For a linearly polarized incident light with frequency ω, the mode transmission matrix can be obtained under the Weisskopf-Wigner approximation. The transmission matrix of guided modes

$$N_g = \pi \sum_k \boldsymbol{E}_g \boldsymbol{E}_g^* \delta(\omega_k - \omega) = \frac{\hbar\omega|\boldsymbol{u}(\boldsymbol{\rho})|^2}{2\varepsilon_0\varepsilon_1 v_g}\hat{\boldsymbol{e}}_z\hat{\boldsymbol{e}}^*{}_z; \tag{B1}$$

here $\sum_k \hat{\boldsymbol{e}}_z\hat{\boldsymbol{e}}^*{}_z \to \int \frac{L}{2\pi v_g}\hat{\boldsymbol{e}}_z\hat{\boldsymbol{e}}^*{}_z d\omega_k$. The $\hat{\boldsymbol{e}}_z$ denotes the basis vector of one-dimensional guided modes. For radiation modes

$$N_v = \pi \sum_k \boldsymbol{E}_v \boldsymbol{E}_v^* \delta(\omega_k - \omega) = \frac{\hbar\omega^3}{6\pi\varepsilon_0\varepsilon_1 c^3} I; \tag{B2}$$

here $\sum_k \hat{\boldsymbol{e}}_v\hat{\boldsymbol{e}}_v^* \to \int \frac{V_v\omega_{k_v}^2}{3\pi^2c^3} I d\omega_k$.

$$\begin{aligned}i(p_s + p_d)N &= i(p_s + p_d)(N_g + N_v) \\ &= i\left(\frac{\gamma_{s,0}}{2} - \frac{\gamma_{d,0}}{2(\omega_k - \omega_0)}\right)I \\ &\quad + i\left(\frac{\gamma_{s,1}}{2} - \frac{\gamma_{d,1}}{2(\omega_k - \omega_0)}\right)I.\end{aligned}$$

The spontaneous emission rates $\gamma_{d,0}/2 = |\boldsymbol{P}_{\text{atom}}|^2\omega|\boldsymbol{u}(\boldsymbol{\rho})|^2/2\hbar\varepsilon_0\varepsilon_1 v_g$ and $\gamma_{d,1}/2 = |\boldsymbol{P}_{\text{atom}}|^2\omega^3/6\pi\hbar\varepsilon_0\varepsilon_1 c^3$. Rayleigh scattering rates $\gamma_{s,0} = \alpha\omega|\boldsymbol{u}(\boldsymbol{\rho})|^2/2v_g$ and $\gamma_{s,1} = \alpha\omega^3/6\pi c^3$.

The outputs of transmitted and reflected fields are obtained:

$$a_t^{\text{out}} = \frac{\frac{\gamma_{d,1}}{2}(1 - \xi\Delta\omega) - i\Delta\omega}{\frac{\gamma_{d,0}+\gamma_{d,1}}{2}(1 - \xi\Delta\omega) - i\Delta\omega}a^{\text{in}}, \tag{B3}$$

$$a_r^{\text{out}} = -\frac{\frac{\gamma_{d,0}}{2}(1 - \xi\Delta\omega)}{\frac{\gamma_{d,0}+\gamma_{d,1}}{2}(1 - \xi\Delta\omega) - i\Delta\omega}a^{\text{in}}. \tag{B4}$$

Here $\Delta\omega = \omega - \omega_0$.

The transmission and reflection can be given by

$$\mathcal{T} = \frac{(\frac{\gamma_{d,1}}{2})^2(1 - \xi\Delta\omega)^2 + (\Delta\omega)^2}{\left(\frac{\gamma_{d,0}+\gamma_{d,1}}{2}\right)^2(1 - \xi\Delta\omega)^2 + (\Delta\omega)^2}, \tag{B5}$$

$$\mathcal{R} = \frac{(\frac{\gamma_{d,0}}{2})^2(1 - \xi\Delta\omega)^2}{\left(\frac{\gamma_{d,0}+\gamma_{d,1}}{2}\right)^2(1 - \xi\Delta\omega)^2 + (\Delta\omega)^2}. \tag{B6}$$

APPENDIX C: THE RELATIONSHIP BETWEEN ATOMIC PROPERTY AND EXCITED ELECTRIC FIELD

In the Heisenberg picture, the electric field of the guided modes can be represented by the time-dependent photon operators

$$E^{(+)}(z,t) = E_{\text{in}}^{(+)}(z,t) + \sum_k E_k e^{i(kz-\omega_k t)}\int_{-\infty}^{t} \dot{a}_k(\tau)d\tau; \tag{C1}$$

here the sign of k denotes the direction of mode $\boldsymbol{k}$, and the excited electric field of nanofiber can be given by

$$E_{\text{in}}^{(+)}(z,t) = \sum_k E_k a_k(-\infty)e^{i(kz-\omega_k t)}. \tag{C2}$$

Same as the S-matrix-like theoretical model, we analyze separately the dipole transition of atom and Rayleigh scattering of the nanocrystal. Then, the interference between the two coupling pathways is studied to obtain the relationship between the excited electric field and the atom property.

1. In the absence of Rayleigh scattering

In the absence of Rayleigh scattering, a two-level artificial atom coupled to the guided modes of a nanofiber is firstly studied irrespective of the radiation modes. By utilizing Eq. (C1), the electric field can be obtained:

$$\begin{aligned}E(z,t) &= \sum_k E_k a_k(t)e^{i(kz-\omega_k t)} \\ &= E_{in}(z,t) + i\zeta\sigma_-\left(t - \frac{|z|}{v_g}\right)e^{-i\omega_0[t-(|z|/v_g)]},\end{aligned} \tag{C3}$$

where $\zeta = \frac{\vec{E}_k \cdot (\vec{E}_k^* \cdot \vec{P}^*) L_g}{\hbar v_g}$.

2. In the absence of dipole transition

In the absence of dipole transition, a typical nanocrystal coupled to the guided modes of nanofiber is secondly analyzed irrespective of the radiation modes; the electric field is

$$E(z>0,t) = \sum_{k>0} E_k a_k(t) e^{-i[\omega_k t-(z/v_g)]} + \sum_{k<0} E_k a_k(t) e^{-i[\omega_k t+(z/v_g)]}. \tag{C4}$$

By using Eq. (A1),

$$a_k = a_k(-\infty) - i \sum_{k>0} \int_{-\infty}^{t} g_{kk'} a_{k'}(\tau) e^{i(\omega_k-\omega_{k'})\tau} d\tau. \tag{C5}$$

By substituting Eq. (C5) into Eq. (C4),

$$\begin{aligned} E(z>0,t) &= E_{k>0,\mathrm{in}}(z,t) + E_{k<0,\mathrm{in}}(z,t) \\ &\quad + \frac{i\gamma_{s,0}}{2}\left[E_{k>0}\left(0,t-\frac{z}{v_g}\right)+E_{k<0}\left(0,t-\frac{z}{v_g}\right)\right] \\ &= E_{\mathrm{in}}(z,t) + \frac{i\gamma_{s,0}}{2} E\left(0,t-\frac{z}{v_g}\right). \end{aligned} \tag{C6}$$

Same as Eq. (C6),

$$\begin{aligned} E(0,\tau) &= E_{k>0}(0,\tau) + E_{k<0}(0,\tau) \\ &= E_{k>0,\mathrm{in}}(0,\tau) + \frac{i\gamma_{s,0}}{4} E(0,\tau) \\ &\quad + E_{k<0,\mathrm{in}}(0,\tau) + \frac{i\gamma_{s,0}}{4} E(0,\tau), \end{aligned} \tag{C7}$$

$$E(0,\tau) = \frac{1}{1-\frac{i\gamma_{s,0}}{2}} E_{\mathrm{in}}(0,\tau). \tag{C8}$$

Finally, we can obtain the electric field of point $z>0$ at time t:

$$\begin{aligned} E(z>0,t) &= \frac{1}{1-\frac{i\gamma_{s,0}}{2}} E_{k>0,\mathrm{in}}(z,t) + E_{k<0,\mathrm{in}}(z,t) \\ &\quad + \frac{\frac{i\gamma_{s,0}}{2}}{1-\frac{i\gamma_{s,0}}{2}} E_{k<0,\mathrm{in}}(-z,t). \end{aligned} \tag{C9}$$

The electric field of point $z>0$ at time t originates from the following three parts: (i) the transmitted field of the nanocrystal for incident excited guided modes $k>0$, with transmission coefficient $\frac{1}{1-i\gamma_{s,0}/2}$; (ii) the direct propagation field for incident excited guided modes $k<0$; and (iii) the reflected field of the nanocrystal for incident guided modes $k<0$ with reflection coefficient $\frac{i\gamma_{s,0}/2}{1-i\gamma_{s,0}/2}$.

3. In the presence of Rayleigh scattering and dipole transition

In the presence of Rayleigh scattering and dipole transition, for convenience, we analyze a two-level artificial atom embedded in a nanocrystal coupled to the fiber modes (guided and radiation modes), by the following Hamiltonian:

$$H = H_0 + H_1, \tag{C10}$$

$$H_0 = \frac{1}{2}\hbar\omega_0\sigma_z + \sum_k \hbar\omega_k a_k^\dagger a_k + \sum_v \hbar\omega_v b_v^\dagger b_v, \tag{C11}$$

$$H_1 = \sum_k \hbar(G_k a_k^\dagger \sigma_- + \mathrm{H.c.}) + \sum_v \hbar(G_v b_v^\dagger \sigma_- + \mathrm{H.c.}), \tag{C12}$$

$$\begin{aligned} H_2 &= \sum_{kk'} \hbar g_{kk'} a_k^\dagger a_{k'} + \sum_{vv'} \hbar g_{vv'} b_v^\dagger b_{v'} \\ &\quad + \sum_{kv} \hbar(g_{kv} a_k^\dagger b_v + \mathrm{H.c.}), \end{aligned} \tag{C13}$$

where a_k ($a_k^\dagger$) denotes annihilation (creation) operators of the guided mode, and b_v ($b_v^\dagger$) denotes annihilation (creation) operators of radiation mode. The coupling strength $G_k = -\frac{1}{\hbar}\boldsymbol{E}_k^* \cdot \boldsymbol{P}_{\mathbf{atom}}{}^*$, $G_v = -\frac{1}{\hbar}\boldsymbol{E}_v^* \cdot \boldsymbol{P}_{\mathbf{atom}}{}^*$, $g_{kk'} = -p_s \boldsymbol{E}_k^* \cdot \boldsymbol{E}_k'$, $g_{vv'} = -p_s \boldsymbol{E}_v^* \cdot \boldsymbol{E}_{v'}$, and $g_{kv} = -p_s \boldsymbol{E}_k^* \cdot \boldsymbol{E}_v$. The $\boldsymbol{E}_k$ and $\boldsymbol{E}_v$ represent the amplitude of guided modes and radiation vacuum modes, respectively.

Under weak-field limit, the equations of motion are

$$\begin{aligned} \dot{a}_k &= -i \sum_{k'} g_{kk'} a_{k'} e^{i(\omega_k-\omega_{k'})t} - iG_k\sigma_- e^{i(\omega_k-\omega_0)t} \\ &\quad - i \sum_v g_{kv} b_v e^{i(\omega_k-\omega_v)t}, \end{aligned} \tag{C14}$$

$$\begin{aligned} \dot{b}_v &= -i \sum_{v'} g_{vv'} b_{v'} e^{i(\omega_v-\omega_{v'})t} - iG_v\sigma_- e^{i(\omega_v-\omega_0)t} \\ &\quad - i \sum_v g_{kv} a_k e^{i(\omega_v-\omega_k)t}, \end{aligned} \tag{C15}$$

$$\dot{\sigma}_- = -\sum_k iG_k^* a_k e^{-i(\omega_k-\omega_0)t} - \sum_v iG_v^* b_v e^{-i(\omega_v-\omega_0)t}. \tag{C16}$$

Formal integration of b_v gives

$$b_v = b_v(-\infty) + \int_{-\infty}^{t} \dot{b}_v(\tau) d\tau = \int_{-\infty}^{t} \dot{b}_v(\tau) d\tau; \tag{C17}$$

here $b_v(-\infty)$ is a noise operator, which can be neglected. To simplify the discussion, we assume that the direction of the dipole is parallel to the electric field, and the near-resonant light of different frequencies has the same field distribution. By utilizing Eq. (C14) ($\dot{a}_k = A_1 + B_1 + C_1$ in turn for convenience) and Eq. (C17), we can obtain

$$\begin{aligned} C_1 &= -i \sum_v g_{kv} b_v e^{i(\omega_k-\omega_v)t} \\ &= -i \sum_v g_{kv} e^{i(\omega_k-\omega_v)t} \int_{-\infty}^{t} \dot{b}_v(\tau) d\tau \\ &= \frac{i\gamma_{s,1}}{2}\Big[-i \sum_{k'} g_{kk'} a_{k'} e^{i(\omega_k-\omega_{k'})t} \end{aligned}$$

$$- iG_k\sigma_- e^{i(\omega_k-\omega_0)t} - i\sum_v g_{kv}b_v e^{i(\omega_k-\omega_v)t}\Big]$$

$$= \frac{i\gamma_{s,1}}{2}(A_1+B_1+C_1). \tag{C18}$$

Thus, we can obtain $\dot{a}_k = \frac{1}{1-i\gamma_{s,1}/2}(A_1+B_1)$.

By using the above formula and Eq. (C1), the electric field of guided modes can be given as

$$\begin{aligned} E(z,t) &= \sum_k E_k a_k(t) e^{i(kz-\omega_k t)} \\ &= E_{\rm in}(z,t) + \frac{1}{1-\frac{i\gamma_{s,1}}{2}} i\zeta\sigma_-\left(t-\frac{|z|}{v_g}\right)e^{-i\omega_0[t-(|z|/v_g)]} \\ &\quad + \frac{1}{1-\frac{i\gamma_{s,1}}{2}}\frac{i\gamma_{s,0}}{2}E\left(0,t-\frac{|z|}{v_g}\right) \\ &= A_2+B_2+C_2. \end{aligned} \tag{C19}$$

Therefore, we can obtain the $E(0,t-\frac{|z|}{v_g})$ by using the above formula,

$$\begin{aligned} E\left(0,t-\frac{|z|}{v_g}\right) =& E_{\rm in}\left(0,t-\frac{|z|}{v_g}\right) \\ &+ \frac{1}{1-\frac{i\gamma_{s,1}}{2}}\left[i\zeta\sigma_-\left(t-\frac{|z|}{v_g}\right)e^{-i\omega_0[t-(|z|/v_g)]}\right. \\ &\left. + \frac{i\gamma_{s,0}}{2}E\left(0,t-\frac{|z|}{v_g}\right)\right]. \end{aligned} \tag{C20}$$

For the transmitted field ($kz \geqslant 0$) of the nanocrystal, $E_{\rm in}(0,t-\frac{|z|}{v_g}) = E_{\rm in}(z,t)$,

$$C_2 = \frac{1}{1-\frac{i\gamma_{s,1}}{2}}\frac{i\gamma_{s,0}}{2}(A_2+B_2+C_2), \tag{C21}$$

$$C_2 = \frac{\frac{i\gamma_{s,0}}{2}}{1-\frac{i(\gamma_{s,1}+\gamma_{s,0})}{2}}(A_2+B_2). \tag{C22}$$

The transmitted field of the solid-state emitter ($kz \geqslant 0$)

$$\begin{aligned} E(z,t) &= \frac{1-\frac{i\gamma_{s,1}}{2}}{1-\frac{i(\gamma_{s,1}+\gamma_{s,0})}{2}}(A_2+B_2) \\ &= \frac{1-\frac{i\gamma_{s,1}}{2}}{1-\frac{i(\gamma_{s,1}+\gamma_{s,0})}{2}}E_{\rm in}(z,t) \\ &\quad + \frac{1}{1-\frac{i(\gamma_{s,1}+\gamma_{s,0})}{2}} i\zeta\sigma_-\left(t-\frac{|z|}{v_g}\right)e^{-i\omega_0[t-(|z|/v_g)]}. \end{aligned} \tag{C23}$$

In the presence of both the dipole transition and Rayleigh scattering, the relationship between the atomic property σ_- and the excited electric field can be obtained by the same method as Eqs. (C14)–(C23),

$$\dot{\sigma}_- = d_0 E_{\rm in}^{(+)}(0,0)e^{-i\Delta\omega t} + d_1\sigma_-, \tag{C24}$$

where $d_0 = \frac{i|\boldsymbol{P}_{\rm atom}|/\hbar}{1-i(\gamma_{s,1}+\gamma_{s,0})/2}$, $d_1 = -\frac{(\gamma_{d,0}+\gamma_{d,1})/2}{1-i(\gamma_{s,1}+\gamma_{s,0})/2}$.

By solving Eq. (C24), we can obtain

$$\sigma_- = i\frac{|\boldsymbol{P}_{\rm atom}|/\hbar}{\frac{\gamma_{d,0}+\gamma_{d,1}}{2}(1-\xi\Delta\omega)-i\Delta\omega}E_{\rm in}^{(+)}(0,0)e^{-i(\omega_k-\omega_0)t}. \tag{C25}$$

APPENDIX D: THE SECOND-ORDER AUTOCORRELATION FUNCTIONS OF OUTPUT FIELDS

We can obtain the transmitted field ($kz > 0$) in the presence of both the Rayleigh scattering and dipole transition, by Eqs. (C23) and (C25),

$$\begin{aligned} E(z,t) &= \frac{1-\frac{i\gamma_{s,1}}{2}}{1-\frac{i(\gamma_{s,1}+\gamma_{s,0})}{2}}E_{\rm in}(z,t) + \frac{1}{1-\frac{i(\gamma_{s,1}+\gamma_{s,0})}{2}} i\zeta e^{-i\omega_0[t-(|z|/v_g)]}\sigma_-\left(t-\frac{|z|}{v_g}\right) \\ &= \frac{1-\frac{i\gamma_{s,1}}{2}}{1-\frac{i(\gamma_{s,1}+\gamma_{s,0})}{2}}E_{\rm in}(z,t) - \frac{\frac{\gamma_{d,0}}{2}}{1-\frac{i(\gamma_{s,1}+\gamma_{s,0})}{2}}\frac{1}{\frac{\gamma_{d,0}+\gamma_{d,1}}{2}-i\delta\omega(1-\frac{i(\gamma_{s,1}+\gamma_{s,0})}{2})}E_{\rm in}(z,t) \\ &= \frac{\frac{\gamma_s}{2}(1-\xi\Delta\omega)-i\Delta\omega}{\frac{\gamma_0+\gamma_s}{2}(1-\xi\Delta\omega)-i\Delta\omega}E_{\rm in}(z,t). \end{aligned} \tag{D1}$$

In the same way, the reflected field ($kz < 0$) can be obtained:

$$\begin{aligned} E(z,t) &= \frac{\frac{i\gamma_{s,0}}{2}}{1-\frac{i(\gamma_{s,1}+\gamma_{s,0})}{2}}E_{\rm in}(z,t) + \frac{1}{1-\frac{i(\gamma_{s,1}+\gamma_{s,0})}{2}} i\zeta e^{-i\omega_0[t-(|z|/v_g)]}\sigma_-\left(t-\frac{|z|}{v_g}\right) \\ &= \frac{\frac{i\gamma_{s,0}}{2}}{1-\frac{i(\gamma_{s,1}+\gamma_{s,0})}{2}}E_{\rm in}(z,t) - \frac{\frac{\gamma_{d,0}}{2}}{1-\frac{i(\gamma_{s,1}+\gamma_{s,0})}{2}}\frac{1}{\frac{\gamma_{d,0}+\gamma_{d,1}}{2}-i\delta\omega(1-\frac{i(\gamma_{s,1}+\gamma_{s,0})}{2})}E_{\rm in}(z,t) \\ &= -\frac{\frac{\gamma_{d,0}}{2}(1-\xi\Delta\omega)}{\frac{\gamma_{d,0}+\gamma_{d,1}}{2}(1-\xi\Delta\omega)-i\Delta\omega}E_{\rm in}(z,t). \end{aligned} \tag{D2}$$

The output fields are consistent with Eqs. (B3) and (B4) of the S-matrix-like theoretical model.

The output fields can be decomposed into the contribution from two parts: (i) the classical field including the incident field and nanocrystal-induced scattering field; and (ii) the nonclassical field induced by atomic dipole transition.

$$E(z,t) = \eta E_{\text{in}} + \beta\sigma_{-}. \tag{D3}$$

The contributions of the classical field to the transmitted and reflected fields are $\eta_{\mathcal{T}} = \frac{1-\frac{i\gamma_{s,1}}{2}}{1-\frac{i(\gamma_{s,1}+\gamma_{s,0})}{2}}$ and $\eta_{\mathcal{R}} = \frac{\frac{i\gamma_{s,0}}{2}}{1-\frac{i(\gamma_{s,1}+\gamma_{s,0})}{2}}$, respectively. The contribution of the nonclassical field induced by atomic dipole transition to the output fields is $\beta\sigma_{-} = -\frac{\frac{\gamma_{d,0}}{2}}{1-\frac{i(\gamma_{s,1}+\gamma_{s,0})}{2}} \frac{1}{\frac{\gamma_{d,0}+\gamma_{d,1}}{2}-i\delta\omega(1-\frac{i(\gamma_{s,1}+\gamma_{s,0})}{2})} E_{\text{in}} = \mu E_{\text{in}}$.

For coherent incident light, by substituting Eq. (D3) into the definition of the second-order correlation function and utilizing $\sigma_{+}^2 = \sigma_{-}^2 = 0$ (Ref. [28]), we can obtain the second-order autocorrelation function

$$g^{(2)} = \frac{\langle E^- E^- E^+ E^+ \rangle}{\langle E^- E^+ \rangle \langle E^- E^+ \rangle} = \frac{|\eta^2 + 2\eta\mu|^2}{|\eta+\mu|^4}. \tag{D4}$$

[1] D. E. Chang, J. I. Cirac, and H. J. Kimble, Phys. Rev. Lett. **110**, 113606 (2013); J. S. Douglas, H. Habibian, C. L. Hung, A. V. Gorshkov, H. J. Kimble, and D. E. Chang, Nat. Photonics **9**, 326 (2015); A. Goban, C.-L. Hung, S.-P. Yu, J. D. Hood, J. A. Muniz, J. H. Lee, M. J. Martin, A. C. McClung, K. S. Choi, D. E. Chang, O. Painter, and H. J. Kimble, Nat. Commun. **5**, 3808 (2014).

[2] E. Vetsch, D. Reitz, G. Sagué, R. Schmidt, S. T. Dawkins, and A. Rauschenbeutel, Phys. Rev. Lett. **104**, 203603 (2010); R. Mitsch, C. Sayrin, B. Albrecht, P. Schneeweiss, A. D. Stone, and A. Rauschenbeutel, Nat. Commun. **5**, 5713 (2014).

[3] H.J. Kimble, Nature (London) **453**, 1023 (2008).

[4] H. Nha, and W. Jhe, Phys. Rev. A **56**, 2213 (1997).

[5] V. V. Klimov, and M. Ducloy, Phys. Rev. A **62**, 043818 (2000).

[6] V. V. Klimov, and M. Ducloy, Phys. Rev. A **69**, 013812 (2004).

[7] F. Le Kien, V. I. Balykin, and K. Hakuta, Phys. Rev. A **73**, 013819 (2006).

[8] F. Le Kien, S. Dutta Gupta, V. I. Balykin, and K. Hakuta, Phys. Rev. A **72**, 032509 (2005).

[9] J. T. Shen and S. Fan, Phys. Rev. Lett. **95**, 213001 (2005).

[10] J. T. Shen and S. Fan, Opt. Lett. **30**, 2001 (2005).

[11] J. Ruostekoski and J. Javanainen, Phys. Rev. Lett. **117**, 143602 (2016).

[12] Z. Liao, X. Zeng, S.-Y. Zhu, and M. S. Zubairy, Phys. Rev. A **92**, 023806 (2015).

[13] A. Goban, C.-L. Hung, J. D. Hood, S.-P. Yu, J. A. Muniz, O. Painter, and H. J. Kimble, Phys. Rev. Lett. **115**, 063601 (2015).

[14] P. Lodahl, S. Mahmoodian, and S. Stobbe, Rev. Mod. Phys. **87**, 347 (2015).

[15] L. Shao, M. Zhang, M. Markham, A. M. Edmonds, and M. Lončar, Phys. Rev. Appl. **6**, 064008 (2016).

[16] T. Aoki, Nature (London) **443**, 671 (2006).

[17] H. Clevenson, M. E. Trusheim, C. Teale, T. Schröder, D. Braje, and D. Englund, Nat. Phys. **11**, 393 (2015).

[18] P. Michler, A. Kiraz, C. Becher, W. V. Schoenfeld, P. M. Petroff, L. Zhang, E. Hu, and A. Imamoglu, Science **290**, 2282 (2000).

[19] A. Laucht, S. Pütz, T. Günthner, N. Hauke, R. Saive, S. Frédérick, M. Bichler, M.-C. Amann, A. W. Holleitner, M. Kaniber, and J. J. Finley, Phys. Rev. X **2**, 011014 (2012).

[20] A. Thoma, P. Schnauber, M. Gschrey, M. Seifried, J. Wolters, J.-H. Schulze, A. Strittmatter, S. Rodt, A. Carmele, A. Knorr, T. Heindel, and S. Reitzenstein, Phys. Rev. Lett. **116**, 033601 (2016).

[21] C. Santori, D. Vučković, G. S. Solomon, and Y. Yamamoto, Nature (London) **419**, 594 (2002).

[22] S. L. Portalupi, G. Hornecker, V. Giesz, T. Grange, A. Lemaître, J. Demory, I. Sagnes, N. D. Lanzillotti-Kimura, L. Lanco, A. Auffèves, and P. Senellart, Nano Lett. **15**, 6290 (2015).

[23] I. Aharonovich, D. Englund, and M. Toth, Nat. Photonics **10**, 631 (2016).

[24] A. Mazzei, S. Götzinger, L. de S. Menezes, G. Zumofen, O. Benson, and V. Sandoghdar, Phys. Rev. Lett. **99**, 173603 (2007).

[25] S. Wang, X. Pan, and L. Tong, Opt. Commun. **276**, 293 (2007).

[26] X.-C. Yu, B.-B. Li, P. Wang, L. Tong, X.-F. Jiang, L. Yan, Q. Gong, and Y.-F. Xiao, Adv. Mater. **26**, 7462 (2014).

[27] X.-C. Yu, Y.-C. Liu, M.-Y. Yan, W.-L. Jin, and Y.-F. Xiao, Phys. Rev. A **86**, 043833 (2012).

[28] Y.-C. Liu, Y.-F. Xiao, B.-B. Li, X.-F. Jiang, Y. Li, and Q. Gong, Phys. Rev. A **84**, 011805 (2011).

[29] E. Waks, and J. Vuckovic, Phys. Rev. Lett. **96**, 153601 (2006).

[30] X. Qi, B. Q. Baragiola, P. S. Jessen, and I. H. Deutsch, Phys. Rev. A **93**, 023817 (2016).

[31] D. Jackson, *Classical Electrodynamics* (Wiley, New York, 1999).

[32] T. Shi, D. E. Chang, and J. I. Cirac, Phys. Rev. A **92**, 053834 (2015).

[33] A. D. Greentree, J. Salzman, S. Prawer, and L. C. L. Hollenberg, Phys. Rev. A **73**, 013818 (2006).

[34] F. Jelezko, and J. Wrachtrup, Phys. Status Solidi A **203**, 3207 (2006).

[35] A. Batalov, C. Zierl, T. Gaebel, P. Neumann, I.-Y. Chan, G. Balasubramanian, P. R. Hemmer, F. Jelezko, and J. Wrachtrup, Phys. Rev. Lett. **100**, 077401 (2008).

[36] R. E. Hummel, *Electronic Properties of Materials* (Springer-Verlag, Berlin, 2001).

[37] V. V. Klimov, M. Ducloy, and V. S. Letokhov, Eur. Phys. J. D **20**, 133 (2002).